Research Paper

Accounting for ground motion directionality and building orientations in urban seismic risk analysis

Earthquake Spectra
XX(X):1–22

DOI: 10.1177/87552930251315751
www.sagepub.com/
SAGE

Alan Poulos,[1] M.EERI, and Eduardo Miranda,[1] M.EERI

Abstract

Regional seismic risk analysis methods are used to estimate the loss of a group of buildings subjected to earthquakes. Buildings usually have two perpendicular horizontal principal orientations, which tend to be similar among buildings within the same city due to the grid-like nature of street layouts. Current regional seismic risk analysis methods do not consider these building orientations to estimate losses because they usually consider orientation-independent measures of horizontal ground motion intensity. However, horizontal ground motions present directionality, meaning that their intensities vary with horizontal orientation. Thus, the response of a building depends on its orientation relative to the orientation of the ground motion. This work studies the effect of building orientations and ground motion directionality on groups of buildings within a city. A testbed group of buildings subjected to an example earthquake is used to estimate losses in terms of the aggregate repair cost of the buildings. The variance of these output losses is shown to be maximized when all buildings share the same principal orientations and minimized when these orientations are fully randomized. A variance-based sensitivity analysis is then performed to compare the contribution to the output variance of ground motion directionality with that of some other sources of uncertainty usually considered in regional seismic risk analyses. When buildings share the same principal orientations and the median ground motion intensities from all orientations are fixed, ground motion directionality is found to be an important source of uncertainty, and its importance increases as more buildings are considered in the analysis. These results suggest that considering ground motion directionality and building orientations could be important for future urban seismic risk analyses and that, under the same seismic hazard, the seismic risk of cities with regular orthogonal street arrangements is larger than that of cities with more irregular street layouts.

Keywords

Directionality, ground motion intensity, urban seismic risk, tall buildings, building orientations

Prepared using sagej.cls *[Version: 2017/01/17 v1.20]*

Introduction

Regional seismic risk analysis estimates the losses or performance of spatially distributed structures when subjected to earthquake events. A critical step in this assessment is estimating the response or damage of a structure given the ground motion at the site, which is usually characterized using horizontal ground motion intensity measures, such as spectral accelerations. This intensity measure varies significantly within the horizontal plane with changes in azimuth, a phenomenon known as ground motion directionality. Several studies have shown that the maximum spectral acceleration in the horizontal plane tends to be significantly larger than other measures of horizontal spectral acceleration (e.g., Beyer and Bommer 2006; Watson-Lamprey and Boore 2007; Huang et al. 2008; Bradley and Baker 2015). For example, spectral accelerations at 1 s are, on average, approximately 55% higher in the orientation of maximum spectral response than in the perpendicular orientation, and this percentage reaches 102% for spectral accelerations at 10 s (Poulos et al. 2022).

Due to the arrangement of lateral load-resisting elements and their geometry in plan and elevation, most buildings have two principal horizontal orientations that are perpendicular to each other (e.g., the longitudinal and transverse axes of a structure), leading to orientation-dependent structural properties. Thus, the response of these buildings to earthquake loading depends on their orientation relative to the ground motions, whose intensities vary significantly with horizontal orientation, and therefore their seismic risk is affected by ground motion directionality.

Groups of buildings within a city tend to have common principal orientations. This is because building orientations tend to follow the orientations of streets, which, for many cities around the world, are primarily arranged in orthogonal grids (Boeing 2019). Moreover, the orientations of maximum horizontal spectral acceleration, typically referred to as RotD100 (Boore 2010), at sites that are close to each other tend to be similar, especially for long periods (Filippitzis et al. 2021; Poulos and Miranda 2023a), leading to significant correlations between the spectral accelerations experienced by buildings in the principal orientations. This, in turn, correlates the responses and the losses between buildings, which increases the variance in the aggregate losses of a group of buildings. This effect is similar to that of other correlations considered in regional seismic risk, such as the spatial correlation of ground motion intensity (Park et al. 2007; Goda and Hong 2008) and the correlation of structural damage (Lee and Kiremidjian 2007; Heresi and Miranda 2022). Neglecting this increase in variance can lead to an underestimation of seismic risk particularly at long return periods that are of interest to structural engineers and the insurance industry.

Regional seismic risk analysis methods almost always neglect ground motion directionality, probably because (i) ground motion models (GMMs), used by these methods to estimate ground motion intensity, usually provide a scalar intensity representative of all horizontal orientations, such as the median intensity (i.e., RotD50, following the definition of Boore 2010); (ii) the methods used to estimate building response

[1]Department of Civil and Environmental Engineering, Stanford University, Stanford, CA, USA

Corresponding author:
Alan Poulos, Department of Civil and Environmental Engineering, Stanford University, 473 Via Ortega, Stanford, CA 94305, USA.
Email: apoulos@alumni.stanford.edu

Prepared using sagej.cls

or damage (e.g., building fragility curves) also use these types of scalar intensities; and (iii) models to estimate ground motion intensity at specific orientations (e.g., Hong and Goda 2007; Poulos and Miranda 2022, 2023b) have been lacking. Thus, building orientations are currently not considered in seismic risk analyses. In other words, if the orientations of the buildings change, the output structural responses, damage, and losses will not change.

This paper studies the effect of accounting for both ground motion directionality and building orientations when estimating the seismic loss of a group of buildings within a city. The method used to estimate seismic losses starts by sampling RotD50 (median intensity in all horizontal orientations) response spectra at the location of each building. These values are then used to compute realizations of response spectra at the horizontal principal orientations of the building, which are assumed to be perpendicular to each other. The response of the building in both orientations is then estimated using a simplified building model consisting of a continuous beam model. These responses are then used to estimate structural and non-structural damage throughout the building and its overall repair cost. The sum of normalized repair costs from all buildings is then used as the output loss variable that quantifies the seismic risk of the group of buildings in the urban area of interest. The method is applied to a group of high-rise buildings arranged in a two-dimensional grid subjected to an example earthquake scenario. Building orientations are considered to have various levels of commonality, varying from a case where the orientation of each building is entirely random to one where all buildings share the same orientations, in order to study its effect on the variance of the total loss of the group of buildings. Finally, a variance-based sensitivity analysis is conducted to evaluate and compare the uncertainty introduced by considering ground motion directionality in the analysis relative to some of the other sources of uncertainty usually considered in these types of analyses, such as those related to structural response modeling and the damage of building components.

Methods

The seismic losses of a group of buildings within a city are estimated using the stochastic simulation method shown schematically in Figure 1. The procedure starts by sampling 5%-damped response spectra at all building locations generated by a scenario earthquake. These initial realizations of response spectra at each site correspond to the median value from all horizontal orientations (i.e., RotD50) and are used to sample response spectra at the two principal orientations of each building. The modal periods and damping ratios of each building at its principal orientations are then sampled to compute 5%-damped spectral acceleration ordinates at each mode of vibration by interpolating from the orientation-dependent spectra and then applying period-dependent damping scaling factors. Then, at each principal orientation, interstory drift ratios (IDRs) and peak floor accelerations (PFAs) are computed along the height of the building using a continuous beam model. These structural responses are then used in combination with fragility functions to sample structural and non-structural damage. The damages are then used to compute repair costs by story using story-based loss functions, which are added for all stories of a building. Finally, the losses of all buildings are added and normalized by the replacement cost of the buildings to obtain a single output loss variable, the loss ratio, as a measure of loss of the group of buildings. Many hundreds of realizations are performed to get statistically significant output losses. Each of these steps is explained in more detail in the following sections.

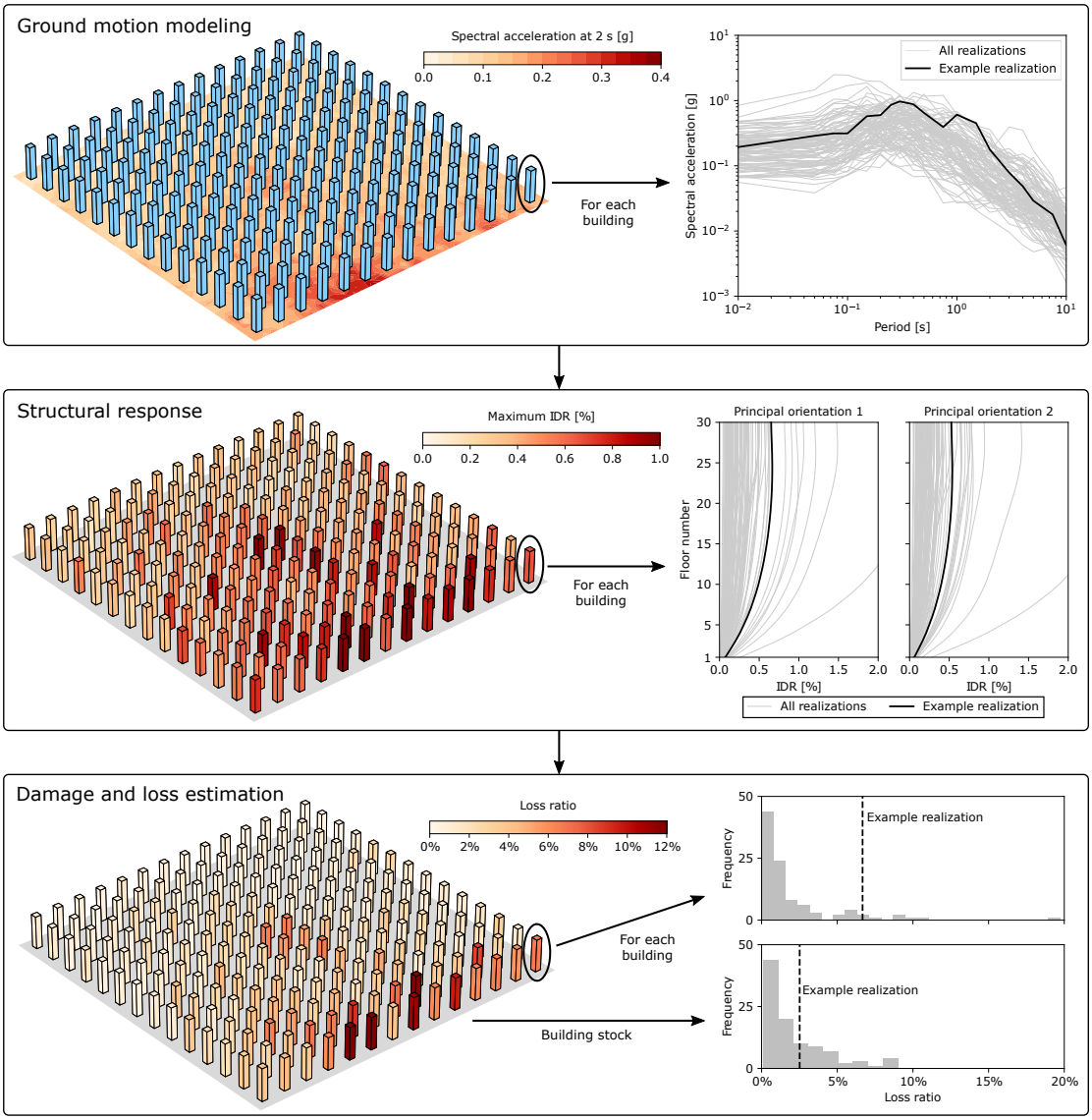

Figure 1. Schematic overview of the regional seismic loss analysis method.

In this study, the method is applied to a group of 196 buildings arranged in a 14x14 grid with a spacing of 200 m. For the sake of simplicity, all buildings are 100 m tall, have 30 stories each, and are steel-braced frame structures. The soil properties are also assumed to be the same for all sites, with an average shear

wave velocity in the top 30 m of soil of 400 m/s. A M_w 7.0 strike-slip earthquake with an epicenter 21 km away from the center of the grid is used as the scenario to compute seismic losses.

Ground motion modeling

The starting point of the simulation is an earthquake scenario, which is defined by a magnitude, rupture surface, and style of faulting. This information, together with site characteristics, is then used as input for the GMM developed by Boore et al. (2014) to obtain realizations of 5%-damped RotD50 response spectra at the location of each building. The sampling considers correlation of spectral ordinates across periods and spatial correlation between response spectral ordinates by using the models developed by Baker and Jayaram (2008) and Heresi and Miranda (2019), respectively.

The GMM of Boore et al. (2014) was developed for the median intensity from all horizontal orientations (i.e., RotD50, following the definition of Boore 2010). However, spectral ordinates can have significant variations with changes in orientation within the horizontal plane. For example, Figure 2a shows the variation of spectral displacement obtained from a linear-elastic single-degree-of-freedom oscillator with a period of 4 s subjected to the horizontal ground motion recorded at the Papanui High School station during the 2010 M_w 7.1 Darfield earthquake. Spectral displacements close to the orientation of maximum intensity (i.e., RotD100) are significantly larger than the RotD50 intensity for this case, whereas spectral intensities at a perpendicular orientation are significantly lower than RotD50. In order to characterize this variation probabilistically, Poulos and Miranda (2022) examined the variation of spectral ordinates as a function of the angular distance to the orientation of RotD100, ϕ, and normalized them by RotD50, introducing the ratio:

$$\nu(\phi) = \frac{Sd(\phi)}{Sd_{\text{RotD50}}}, \qquad \phi \in [0°, 90°] \tag{1}$$

where $Sd(\phi)$ is the spectral displacement at an angular distance of ϕ from the orientation of RotD100 and Sd_{RotD50} is the RotD50 spectral displacement. Please note that, by definition, $\nu(\phi)$ is also the ratio between pseudo-spectral accelerations. This ratio can be computed for several ground motion records, as shown, for example, in Figure 2b for 100 ground motion records. Each ground motion record has two curves, which correspond to intensities produced by clockwise and counterclockwise rotations from the orientation of RotD100. Using more than five thousand ground motion records from the NGA-West2 database, Poulos and Miranda (2022) developed a probabilistic model of ν ratios and fitted beta probability distributions with different combinations of angle ϕ and period.

For the case of buildings with two principal orientations that are perpendicular to each other, response spectra need to be sampled simultaneously at both principal orientations (i.e., P_1 and P_2) to guarantee a correct correlation across sites, periods, and orientations. This can be achieved by following the procedure depicted schematically in Figure 3. The first step is to sample the orientation of RotD100, which, for simplicity, is sampled from a uniform distribution over all horizontal orientations. Other distributions that could be used to sample the orientation of RotD100 are those recently developed by Poulos and Miranda (2023a) for strike-slip earthquakes, which favor the orientation of RotD100 occurring close to the transverse orientation, or the distribution developed by Shahi and Baker (2014) for directivity effects at rupture distances shorter than 5 km, which favor the strike-normal orientation. Once the orientation of RotD100 is known, angular distances ϕ_1 and ϕ_2 between this orientation and the two principal orientations of each building are computed as shown in Figure 3a. Then, the ν ratios are sampled

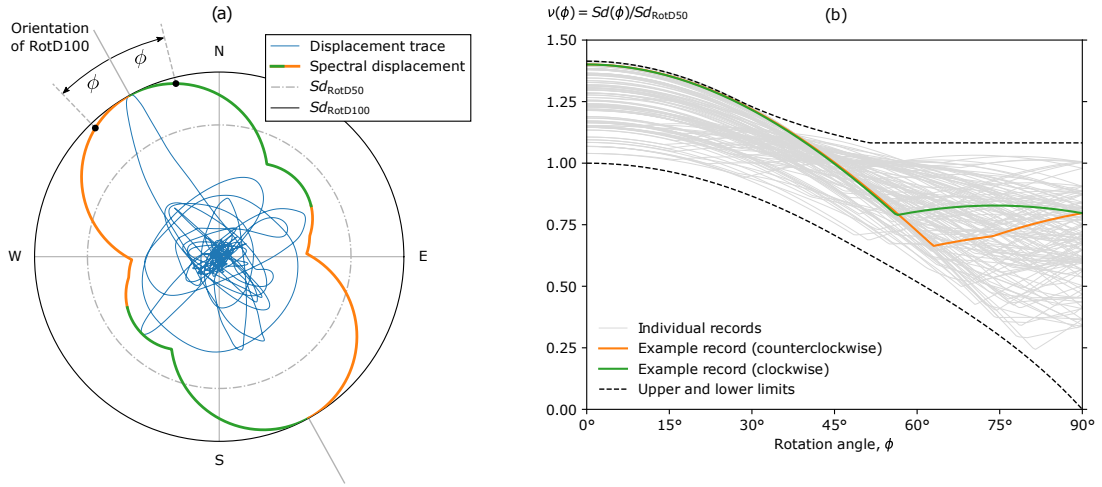

Figure 2. Ground motion directionality of spectral responses at 4 s. (a) Relative displacement hodogram and spectral response as a function of horizontal orientation of an example ground motion recorded during the 2010 M_w 7.1 Darfield earthquake at the Papanui High School station. (b) Ratios between spectral accelerations as a function of the angular distance to the orientation of RotD100 and the median spectral response (RotD50) for 100 example records.

independently for both computed angles at each period using the distribution fitted by Poulos and Miranda (2022), as shown in 3b. Finally, the sampled ν ratios are multiplied by the RotD50 intensities to obtain spectra at both principal orientations of each building, i.e.:

$$Sd_i = \nu(\phi_i) Sd_{\text{RotD50}}, \qquad i \in \{1, 2\} \tag{2}$$

where Sd_1 and Sd_2 are the spectral displacements at each principal orientation. These spectral displacements are computed at all periods of interest using Equation (2). This procedure for sampling ground motion intensity captures the component-to-component variability between different horizontal orientations (e.g., as represented by the σ_c term of Boore et al. 1997), while associating the sampled intensity with the angular distance from the orientation of RotD100.

Structural response

Each building is characterized by modal periods and damping ratios in both principal orientations. In this study, six modes are considered for each principal orientation. These properties are sampled in several steps. First, the fundamental periods and damping ratios are sampled at both orientations using a model developed by Cristian Cruz and Pablo Heresi with data inferred from seismic responses of buildings in California through system identification (Cruz 2017). In this model, the fundamental periods at both principal orientations, $\mathbf{T}^\top = [T_{P1}, T_{P2}]$, are sampled from the following height-dependent expression developed for steel-braced frame buildings:

$$\ln(\mathbf{T}) = a_T + b_T \ln(h) + \sigma_T \boldsymbol{\varepsilon}_T \tag{3}$$

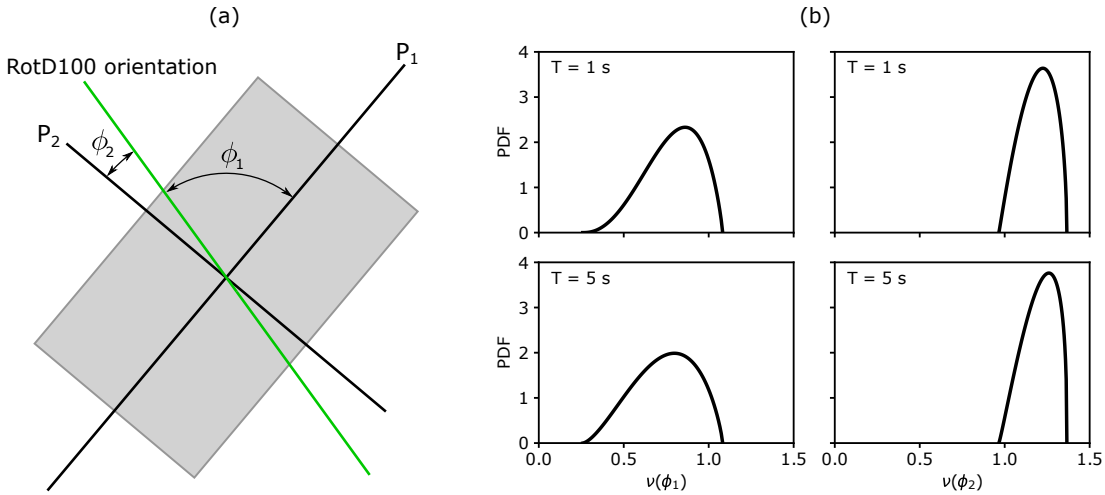

Figure 3. Sampling of ground motion intensities in the principal orientations of a building. (a) Computation of the angular distances between the orientation of RotD100 and both principal orientations of the building. (b) Sampling distributions of ν ratios in the two principal orientations for two example periods of 1 and 5 s, obtained from Poulos and Miranda (2022).

where a_T = -3.4514, b_T = 0.9290, and σ_T = 0.2865 are fitted coefficients; h is the height of the building in meters; and ε_T is sampled from a bivariate normal distribution with zero mean, unit standard deviation, and a correlation coefficient of ρ_T = 0.8926:

$$\varepsilon_T \sim \mathcal{N}_2 \left(\begin{bmatrix} 0 \\ 0 \end{bmatrix}, \begin{bmatrix} 1 & \rho_T \\ \rho_T & 1 \end{bmatrix} \right) \tag{4}$$

The same procedure is followed to sample height-dependent damping ratios for the fundamental mode in both principal orientations:

$$\ln(\boldsymbol{\xi}) = a_\xi + b_\xi \ln(h) + \sigma_\xi \varepsilon_\xi \tag{5}$$

$$\varepsilon_\xi \sim \mathcal{N}_2 \left(\begin{bmatrix} 0 \\ 0 \end{bmatrix}, \begin{bmatrix} 1 & \rho_\xi \\ \rho_\xi & 1 \end{bmatrix} \right) \tag{6}$$

but with different coefficients and correlation: $a_\xi = -1.8606$, $b_\xi = -0.4393$, $\sigma_\xi = 0.2855$, and $\rho_\xi = 0.4058$. Using this sampling procedure, the 100-m buildings analyzed have, on average, fundamental periods of 2.38 s and damping ratios of the fundamental mode of 2.1%.

Higher modal periods and effective mode shapes are obtained using the non-uniform continuous beam model developed by Alonso-Rodríguez and Miranda (2016), which corresponds to a linear elastic shear beam laterally coupled to a linear elastic flexural beam whose lateral stiffness are reduced parabolically and quartically, respectively, with increasing height. The effective mode shapes (i.e., products of mode shapes and participation factors) and period ratios in the model only depend on two non-dimensional parameters, the ratio between the shear and flexural stiffness at the base of the building (α) and the ratio

between the lateral stiffness at the top and base of the building (δ). For this study, α is sampled from a uniform distribution between 0 and 5 for each building, and δ is assumed to be a deterministic function of building height given by:

$$\delta = \max\{0.01, 0.35 - 0.001\ h\} \tag{7}$$

Modal damping ratios at higher modes are obtained from the model developed by Cruz and Miranda (2017), which, for steel-braced frame buildings, has the following form:

$$\xi_j = \xi_1 \left[1 + 0.13\,(T_1/T_j - 1) + 0.44\,\varepsilon\right], \qquad j \in \{2, 3, 4, 5, 6\} \tag{8}$$

where ξ_j and T_j are the damping ratio and period of the j-th mode; and ε is a standard normal random variable. The sampling is performed independently in both principal orientations of the building. Note that this does not mean that damping ratios of higher modes in perpendicular orientations are uncorrelated, because the first translational modal damping ratios are correlated through Equation (5).

After obtaining the dynamic properties of all modes at each principal orientation, the next step is to obtain spectral accelerations that are specific to each mode. This is achieved by first interpolating the 5%-damped response spectrum at the modal periods and then using the damping scaling factors developed by Rezaeian et al. (2014):

$$Sa(T_j, \xi_j) = Sa_{5\%}(T_j) C(T_j, \xi_j) \tag{9}$$

where $Sa(T_j, \xi_j)$ is the spectral acceleration at the j-th mode, $Sa_{5\%}(T_j)$ is the 5%-damped spectral acceleration at the j-th mode obtained from interpolation, and $C(T_j, \xi_j)$ is the damping scaling factor, which is sampled from a lognormal probability distribution:

$$C(T_j, \xi_j) \sim \text{Lognormal}\left(\mu_{\ln C}(T_j, \xi_j), \sigma^2_{\ln C}(T_j, \xi_j)\right) \tag{10}$$

with parameters $\mu_{\ln C}$ and $\sigma_{\ln C}$ being the, respectively, the mean and standard deviation of the logarithm of the scaling factor, which are obtained from Rezaeian et al. (2014).

The final step is to obtain structural responses, in terms of interstory drift ratios (IDRs) and peak floor accelerations (PFAs), along the height of each building from the sampled spectral accelerations of the six modes. This is conducted independently for both principal orientations using modal response spectrum analysis, with the orientation-specific spectral accelerations sampled previously as input. The modal combination rule used for IDRs is the square root of the sum of squares (SRSS), whereas the rule used for PFAs is the complete quadratic combination (CQC) procedure for total accelerations developed by Taghavi and Miranda (2006). A couple of errors were found in the original expressions provided by Taghavi and Miranda (2006), which were corrected by Pablo Heresi. The corrected expressions are presented in the supplemental material for this article.

Damage and loss estimation

Damage and loss estimation is performed using a story-based approach. In this procedure, each building story is populated with a generic inventory of structural and non-structural components that depend on the use of the building, defined by Ramirez and Miranda (2009) for tall buildings. These components are either drift- or acceleration-sensitive, which governs the structural response that affects their damage. Damage states are then sampled using the fragility curves assigned by Ramirez and Miranda (2009) to each type of component. At each story and principal orientation, all components of the same type are

assumed to have the same damage state. Thus, the repair cost of each story can be sampled without knowing the number of components of each type as:

$$l = \frac{1}{2} \sum_{o=1}^{2} \sum_{i=1}^{n_c} p_i \, l_{i,o} \tag{11}$$

where l is the repair cost of a story normalized by the replacement cost of the story; n_c is the number of component types obtained from Ramirez and Miranda (2009); p_i is the proportion of the cost of a story associated with the i-th component type; $l_{i,o}$ is the repair cost of the i-th component type (normalized by its cost) at orientation o, which depends on the sampled damage state of the component (see Tables 3.3-3.5 of Ramirez and Miranda 2009). Since the loss estimation method considers both principal orientations of the building, which was not considered by Ramirez and Miranda (2009), Equation (11) is multiplied by a factor of one-half to be consistent with the total losses of the building, essentially assuming that, at each story, half of the components of each type are sensitive to structural responses at each orientation. Building collapse was not considered in the loss analysis, which is a reasonable assumption for this type of structure and ground motion intensity level. These losses could easily be added to the analysis by considering a building collapse fragility function. Finally, the losses are summed for all stories and buildings and divided by the replacement cost of all buildings to obtain the loss ratio for the complete building set, which is the output variable of the analysis and provides a quantitative measure of loss for the group of buildings.

Sensitivity analysis

Table 1 summarizes the random variables considered in the analysis and specifies their probability distribution. Most of these random variables are sampled several times for the same realization depending on the number of buildings (n_b), periods (n_p), modes (n_m), stories (n_s), and building components (n_c), which in this study take values of 196, 22, 6, 30, and 23, respectively.

Table 1. Random variables considered in the seismic risk analysis.

Random variable	Distribution	Number
RotD100 azimuth	Uniform: $\mathcal{U}(0, \pi)$	1
ν ratios	Beta	$2n_b n_p$
First translational periods	Bivariate normal	$2n_b$
First translational damping ratios	Bivariate normal	$2n_b$
Damping ratios at higher modes	Normal	$2(n_m - 1)n_b$
α ratios	Uniform: $\mathcal{U}(0, 5)$	$2n_b$
Damping scaling factor: C	Lognormal	$2n_b n_m$
Damage states	Categorical	$2n_b n_s n_c$

The variables associated with ground motion directionality, which is almost always neglected by regional seismic risk analysis methods, are the azimuth of RotD100 and the ν ratios. A variance-based sensitivity analysis is performed to compare the effect of these two variables with the effect of the rest of the sources of uncertainty presented in Table 1. The sensitivity to each of the input random variables

(or group of random variables) considered was quantified using the total-effect Sobol index (Homma and Saltelli 1996), which represents the proportion of the variance of the output variable (in this analysis the loss ratio) contributed by each given random variable, including all interactions of any order with the rest of the random variables. This global sensitivity analysis method was selected over local approaches (such as derivative-based or one-at-a-time methods) because it enables a comprehensive exploration of the entire input space, without relying on the arbitrary selection of nominal values. The Sobol indices were computed using a Monte Carlo-based approach (Saltelli et al. 2010), with 500 simulations for each random variable.

Building orientations

This section presents the probability distribution used to sample the principal horizontal orientations of buildings. Buildings are assumed to have two principal orientations that are perpendicular to each other. One of these principal orientations will be at a angular distance less than or equal to $\pi/4$ from the north direction. To model the azimuth of this orientation, which is between $-\pi/4$ and $\pi/4$, we start from a von Mises (circular normal) distribution, a commonly used probability distribution in directional statistics, which has probability density function (PDF):

$$f_\Phi(x;\mu,\kappa) = \frac{\exp\left(\kappa\cos(x-\mu)\right)}{2\pi I_0(\kappa)}, \quad x \in [-\pi,\pi] \tag{12}$$

where I_0 is the modified Bessel function of order 0; and μ and κ are the parameters of the distribution, which represent the mean and a measure of concentration. The von Mises distribution is defined over a range of length 2π because it represents all possible directions. However, a single building orientation has a periodicity of π because two directions at an angular distance of π represent the same orientation (e.g., north and south are the same orientation). Moreover, because we are assuming that the principal building orientations are perpendicular to each other, one of these orientations will be within a range of length $\pi/2$. We can therefore construct a new probability distribution by adding the probability density function of the von Mises distribution at four angles with $\pi/2$ spacing as follows:

$$f_A(x;\mu,\kappa) = f_\Phi(x;\mu,\kappa) + f_\Phi(x+\pi/2;\mu,\kappa) + f_\Phi(x+\pi;\mu,\kappa) + f_\Phi(x+3\pi/2;\mu,\kappa) \tag{13}$$

$$= \frac{\cosh(\kappa\cos(x-\mu)) + \cosh(\kappa\sin(x-\mu))}{\pi I_0(\kappa)}, \quad x \in [-\pi/4,\pi/4] \tag{14}$$

This distribution is then combined with a uniform distribution through a weighted sum to better fit with empirical street data of different cities:

$$f_B(x;\mu,\kappa,\omega) = \omega f_A(x;\mu,\kappa) + (1-\omega) f_U(x), \quad x \in [-\pi/4,\pi/4] \tag{15}$$

where ω is a parameter representing the weight used to combine the two probability distributions, and f_U is the PDF of a uniform distribution:

$$f_U(x) = \frac{2}{\pi}, \quad x \in [-\pi/4,\pi/4] \tag{16}$$

Figure 4a shows the probability distribution used to sample building orientations, f_B, for the case where $\mu = 0°$, $\kappa = 8$, and $\omega = 0.6$, together with both component distributions, f_A and f_U, with their

corresponding weights. Two additional distributions are presented in the figure to illustrate the effect of modifying parameters μ and κ, which shift the mean and increase the concentration around μ, respectively. The three distributions are also presented in a polar representation in Figure 4b to show how they relate to the cardinal directions.

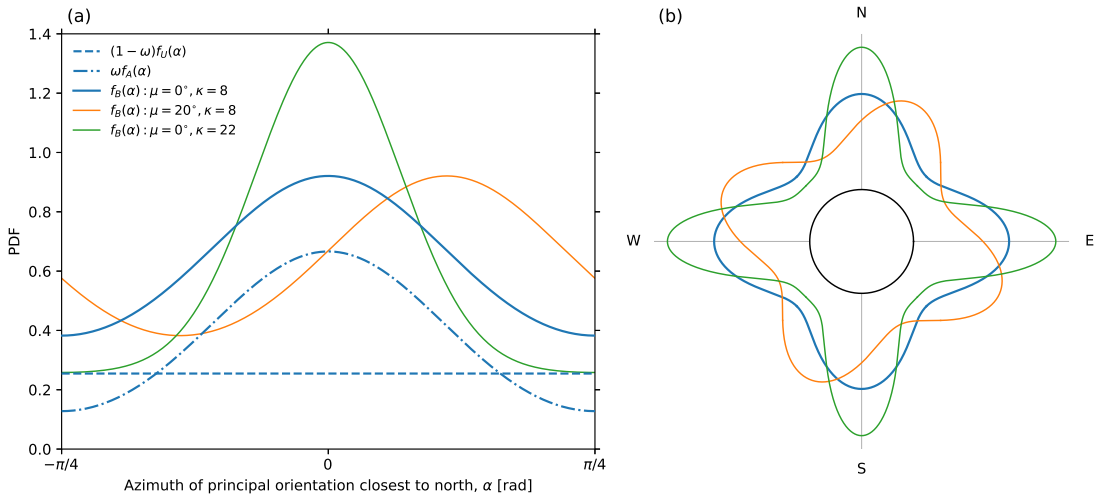

Figure 4. Example probability density functions used to model the azimuth of the building principal orientation closest to north, presented in a (a) linear and (b) polar representation. All distributions shown here have ω = 0.6.

Buildings are usually oriented to follow the orientations of streets. Thus, a global urban street network database developed by Boeing (2022) is used to study the effectiveness of the proposed probability distribution. The database consists of 8,914 urban areas located in 178 countries, all with a population of at least 50,000. For each urban area, the azimuths of each street are transformed to the $[-\pi/4, \pi/4]$ range using the following expression:

$$\psi_f = ((\psi_i + \pi/4) \bmod \pi/2) - \pi/4 \tag{17}$$

where ψ_i is the azimuth of a street, ψ_f is the azimuth of the street transformed to the $[-\pi/4, \pi/4]$ range, and mod is the modulo operator (sometimes also referred to as the remainder operator). Once all azimuths are obtained, a maximum likelihood estimation is used to fit the three parameters of the f_B probability distribution to the data, with further details presented in the supplemental material for this article. As an example, Figure 5 shows the empirical distribution of street azimuths for the cities of Seattle and Mexico City. Seattle has most of its streets very close to the north-south or east-west orientation (i.e., an azimuth of 0°), whereas Mexico City has street orientations that are less concentrated, with a higher-than-average density at an azimuth close to 14.5°, which coincides with the city's most important avenue (i.e., Av. Insurgentes) that runs through the whole city with that azimuth. Figure 5 also shows the fitted distributions, which match the data relatively well for both cities.

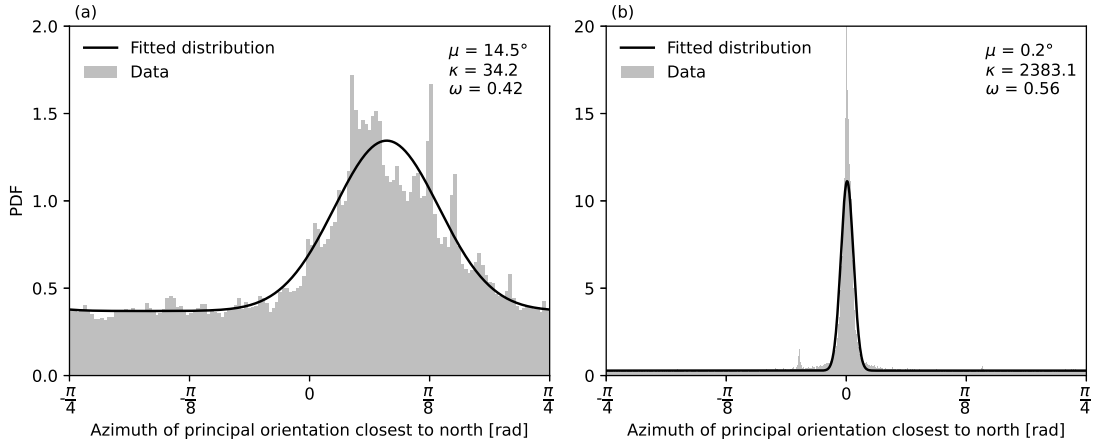

Figure 5. Empirical distribution of the orientations of streets and fitted probability distribution for the (a) Mexico City and (b) Seattle urban areas.

The f_B probability distribution was fitted for all 8,914 urban areas in the Boeing (2022) database, resulting in the κ and ω parameters shown in the scatter plot of Figure 6. Urban areas are color-coded according to the region of the world where they are located. Urban areas in North America tend to have higher values of κ, and hence more concentrated street orientations, than those in other world regions. This is the case for major urban area in the west coast of the United States subjected to significant seismic hazard, such as Seattle, Los Angeles, and the San Francisco Bay Area.

In order to study the effect of building orientations on urban seismic risk analysis, this work considers four different f_B distributions, which are shown in Figure 7. The first three have $\omega = 1$ and $\mu = 0°$ and values of κ being 0, 10, and ∞, which represent distributions that are uniform, significantly concentrated in the north-south orientation, and fully concentrated in the north-south orientation, respectively. The fourth distribution is the one fitted for Mexico City shown in Figure 5a. Samples of building orientations using each of these distributions are shown in Figure 7c-f. These orientations are sampled only once for each case, and hence are not included as a source of uncertainty in Table 1, which presents the variables being sampled for each simulation. In other words, the effects of the various random variables listed in Table 1 are analyzed for four fixed (deterministic) sets of building orientations.

Results

Figure 8 shows the loss ratio computed from 1000 simulations for each of the four considered building groups as a function of the azimuth of RotD100. A general trend of the loss ratio with the azimuth of RotD100 is presented for each case using locally weighted scatterplot smoothing (LOWESS) (Cleveland 1979), which were computed by local weighted linear regressions that used 20% of the simulations whose azimuths of RotD100 were closest to each point. As expected, the azimuth of RotD100 has almost no effect on the total seismic losses for the case where building orientations are sampled using a uniform distribution ($\mu = 0$, $\kappa = 0$), as shown in Figure 8a. When building orientations are sampled

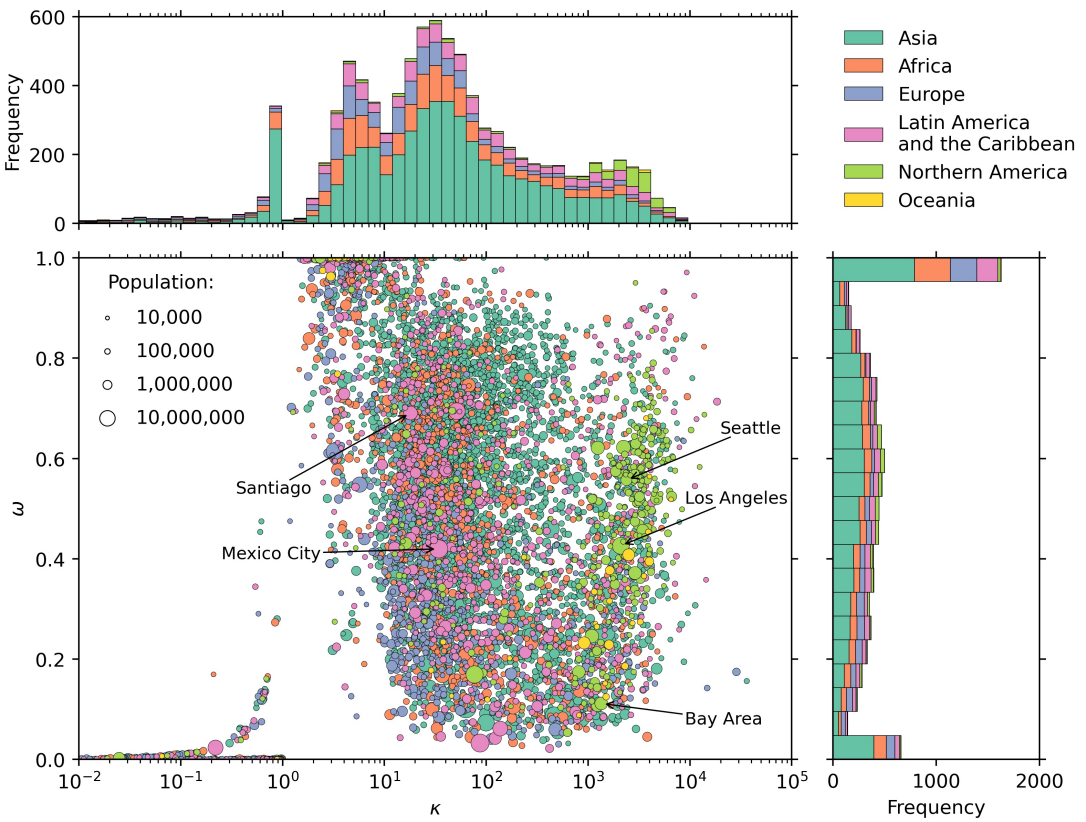

Figure 6. κ and ω parameters of the probability distributions of the orientations of streets fitted for 8,914 urban areas. The color indicates the region of the world where the urban area is located, and the size of the circles indicate its residential population.

with a preferential north-south and east-west orientation (i.e., with $\mu = 0$ and $\kappa = 10$), shown in Figure 8b, the resulting losses vary significantly with changes in the azimuth of RotD100, with the losses being higher, on average, at the north, east (same as west), and south azimuths, where the azimuth of RotD100 is close to one of the principal orientations of the buildings. Moreover, the standard deviation of the losses increases from 0.022% for the uniform case to 0.028%. As shown in Figure 8c, the azimuth of RotD100 affects the total losses even more for the case when all buildings are orientated north-south east-west ($\mu = 0$, $\kappa \to \infty$), and the standard deviation increases to 0.045%. Finally, Figure 8d presents the results for the distribution of building orientations fitted using the Mexico City data, which shows that the azimuth of RotD100 affects the total losses to a similar extent as in the intermediate case of $\kappa = 10$ and also has a very similar standard deviation. However, given that the distribution for Mexico City is shifted by 14.5°, the azimuths where total losses are larger are also shifted by the same amount.

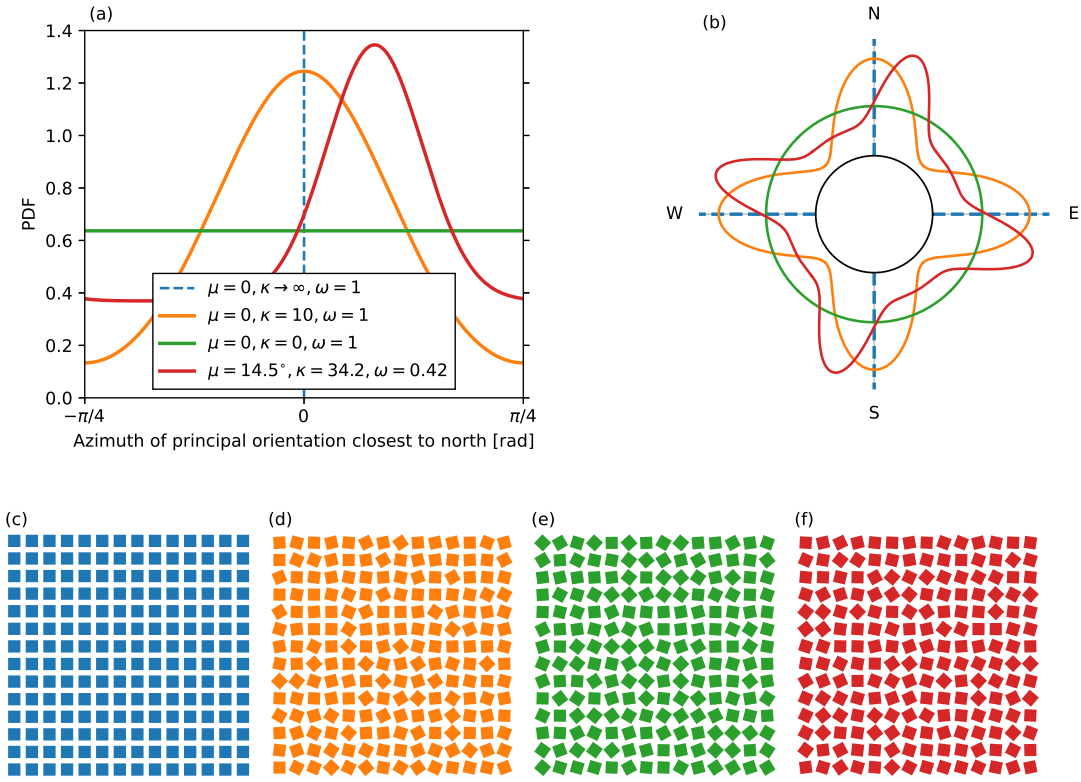

Figure 7. Sampling of building principal orientations. Probability distributions used for sampling in a (a) linear and (b) polar representations. Example orientation samples for the cases of: (c) perfect north-south east-west orientations (d) preferential north-south east-west orientations, (e) random orientation with uniform density, and (f) distribution of azimuths fitted for Mexico City.

In order to compare the uncertainty introduced by the sampling of the RotD100 azimuth with the other sources of uncertainty presented in Table 1, total-effect Sobol indices were computed. These indices quantify the contribution of each variable (or group of variables) to the variance of the output variable. Figure 9a shows the total-effect Sobol indices for the case where the orientations of each building is entirely random with each orientation being equally likely (i.e., with a uniform probability distribution). For this case, the highest contribution to the output variance comes from the variability of the fundamental periods of the buildings. Unsurprisingly, the azimuth of RotD100 has a very low contribution to the output variance, which is consistent with the simulations shown in Figure 8a. The other sources of uncertainty in total losses, namely from variability in damping ratios, ν ratios, damping scaling factors, component damage, and α ratios, also have relatively low Sobol indices.

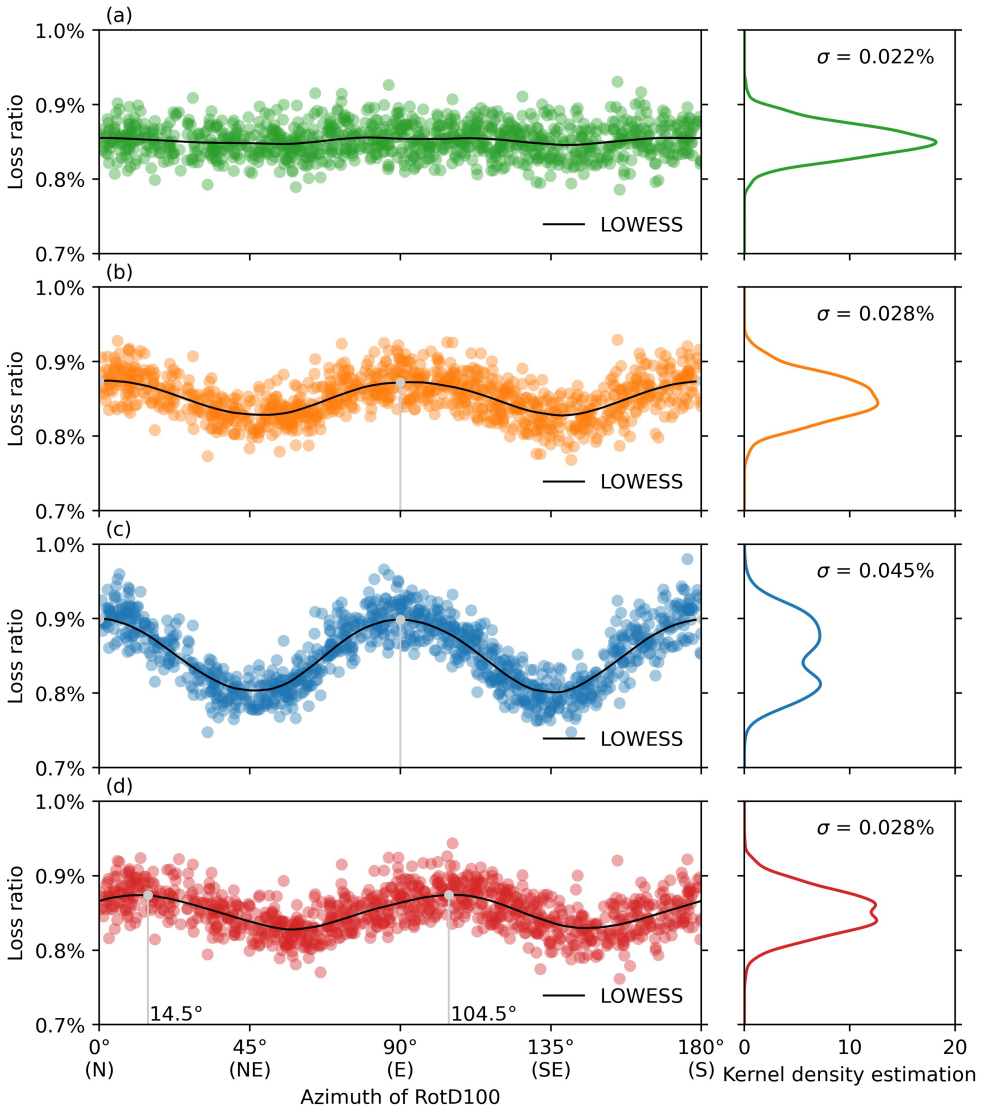

Figure 8. Loss ratio computed from 1000 simulations as a function of the azimuth of RotD100 for the cases when the building grid has: (a) random orientation with uniform density, (b) preferential north-south east-west orientations, (c) perfect north-south east-west orientations for all buildings, and (d) distribution of azimuths fitted for Mexico City. The right panels present a kernel density estimations of the corresponding output variable. Each row also presents the standard deviation of the distribution (σ).

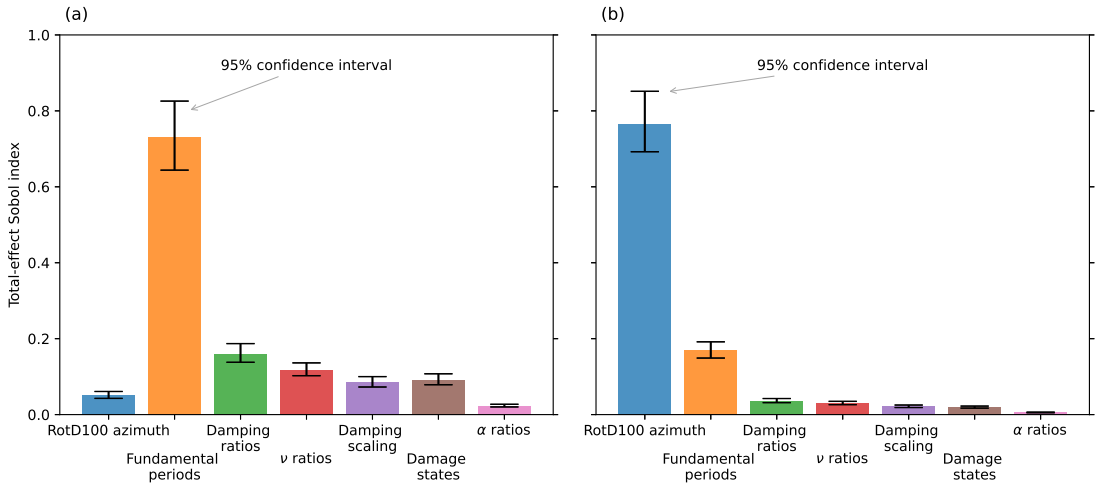

Figure 9. Total-effect Sobol indices of the seven considered random variables for the cases where building have (a) different orientations sampled with uniform density and (b) the same north-south/east-west orientation. Error bars represent 95% confidence intervals estimated using bootstrapping.

Sobol indices for the case where all buildings have the same north-south/east-west orientation are shown in Figure 9b. Now the azimuth of RotD100 has by far the highest contribution to the variance of total losses, with a Sobol index of approximately 0.77. The second group of variables that contribute the most to the variance of total losses are the fundamental periods of the buildings, with a Sobol index of approximately 0.17. The rest of the variables contribute much less to the output variance. Due to the use of a finite number of simulations (i.e., 500 simulations), Figure 9 also shows 95% confidence intervals for each Sobol index, which were computed with bootstrapping using the percentile method (Efron 1982).

The number of buildings used for the simulations plays a significant role in the Sobol indices obtained for the perfectly north-south/east-west case. The testbed consists 196 buildings, with the output losses being the sum of the losses from all buildings. However, using a different number of buildings would alter the results. For example, Figure 10 shows the mean Sobol indices as a function of the number of considered buildings. For each number of buildings, 100 random subsets are selected from the 196 buildings and the sum of the losses are computed for each subset. Sobol indices were then computed for each subset and Figure 10 shows the means of these values. The mean Sobol indices remain stable across the full range of number of buildings for the case of random orientations that are uniformly distributed. However, in the case where all buildings have the same orientation (i.e., north-south/east-west), the Sobol index related to the azimuth of RotD100 increases as more buildings are included in the analysis, with the rest of the Sobol indices decreasing accordingly. This can be explained by the fact that the rest of the random variables are being sampled independently for each buildings, whereas the azimuth of RotD100 introduces a correlation between buildings losses. Because it is assumed that the azimuth of RotD100 is common for all buildings, the angle between this orientation and the principal orientations of all buildings (i.e., ϕ) is also the same in the perfectly north-south/east-west case. Thus, if higher/lower than average

ground motion intensities are sampled for a given building, ground motions at other buildings are likely also higher/lower than average, leading to a dependence of losses between buildings. However, in the case where building orientations are entirely random and uniformly sampled, the ϕ angles are different for all buildings, making building losses practically independent of the azimuth of RotD100.

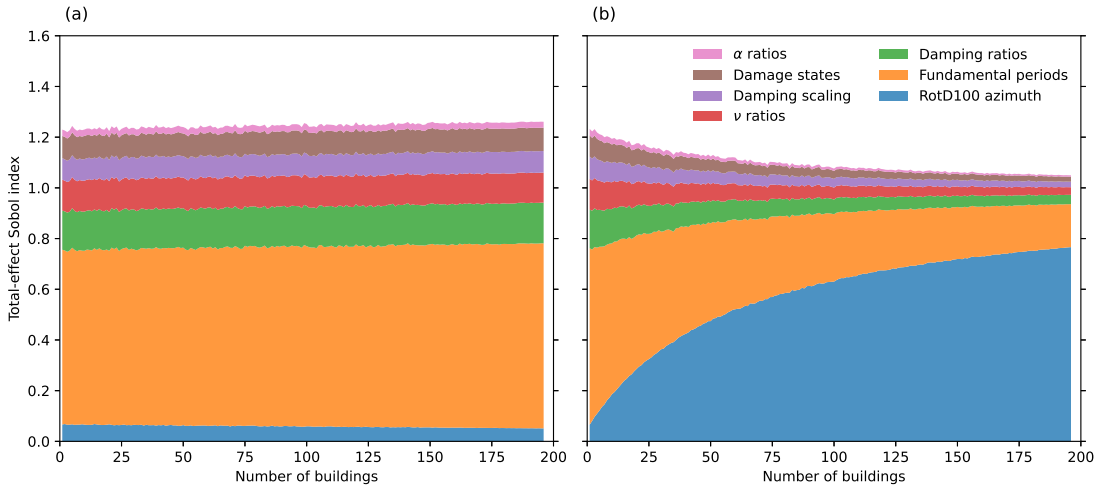

Figure 10. Total-effect Sobol indices of the seven considered random variables as a function of the number of buildings used in the analysis, for the cases where building have (a) different orientations sampled with uniform density and (b) the same north-south/east-west orientation.

All results presented in this study are based on a constant RotD50 ground motion intensity field, initially set to the median intensity from the ground motion model. To examine how variations in intensity affect the results for the case where all buildings have the same orientation, four additional analyses were conducted by adjusting the RotD50 spectral accelerations at each building location. As shown in Figure 11, these adjustments range from subtracting 0.5 standard deviations to adding 1.5 standard deviations (on a logarithmic scale), with increments of 0.5 standard deviations. This results in mean spectral accelerations at 2 s varying from 0.053g to 0.216g. Correspondingly, building losses also show significant variation across the intensity range, with mean loss ratios spanning from 0.41% to 7.48%. Overall, the Sobol indices are similar across the range of ground motion intensities, and the ranking of the importance of the random variables (i.e., the relative importance of each random variable) remains relatively constant, with the azimuth of RotD100 contributing the most to output losses, followed by the fundamental period of the buildings.

The testbed of this study assumes that all buildings have the same height and lateral force-resisting system, which makes their first translational period similar and, therefore, their associated spectral ordinates have higher levels of correlation than they would in a group of buildings with a wider range of heights and lateral force-resisting systems. Moreover, because all buildings have a height of 100 m, their first translational periods are relatively long, where ground motion directionality is more important. The effect of the azimuth of RotD100 on the total losses is expected to be smaller for cases where most

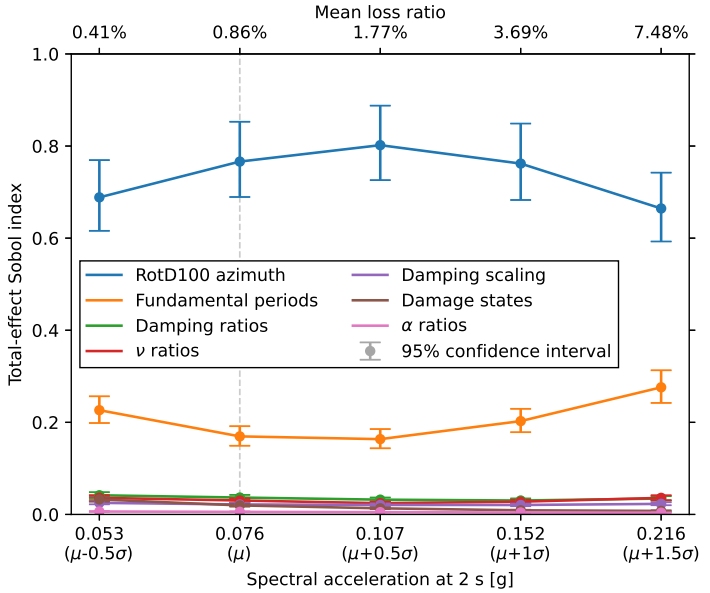

Figure 11. Effect of ground motion intensity, characterized by the spectral acceleration at 2 s, on the total-effect Sobol indices of the seven considered random variables for the case where all buildings have the same north-south/east-west orientation. The bottom axis presents in parentheses the number of standard deviations below or above the median ground motion intensity level and the top axis presents the associated mean loss ratio. Error bars represent 95% confidence intervals of the Sobol indices estimated using bootstrapping. The vertical dashed line indicates the results for the original median ground motion intensities (i.e., Figure 9b).

buildings are low-rise and when the building stock is more heterogeneous. Furthermore, soil properties are assumed to be uniform across all sites. In practice, however, these properties may vary, particularly for larger regions with diverse soil conditions, and could be adjusted using available geotechnical data for the region. Another important assumption of this study is that the orientation of RotD100 is the same for all buildings. While this is expected to be a good assumption for relatively small portions of cities representative of downtown districts, where all or most tall buildings are located, an application to a large urban area also requires consideration of the variation of RotD100 orientations between sites. Finally, peak structural responses in this study are estimated using linear models, which, while relatively accurate for tall buildings subjected to low to medium intensity levels, may be less accurate in other contexts. Future studies could explore the use of nonlinear models with broader applicability, allowing for the incorporation of additional sources of uncertainty, such as yield strength and hysteretic behavior.

Conclusions

This study has developed an approach to explicitly consider the effect of ground motion directionality and building orientations for a group of buildings within a city when performing seismic risk analysis. Since

building principal orientations tend to be parallel and perpendicular to street orientations, which for most cities have somewhat of a grid pattern, a large number of buildings within a city tend to have the same or similar orientations. Ground motion intensity varies with changes in horizontal orientation, and the orientations of maximum ground motion intensity (RotD100) are also fairly similar for sites close to each other, especially for long periods. Thus, losses will tend to be higher when the orientation of RotD100 coincides or is close to one of the principal orientations of the buildings and will tend to be lower when the orientation of RotD100 is farther away from the principal orientations of the buildings in the city. Consequently, the losses between buildings tend to be correlated due to ground motion directionality.

The effect of ground motion directionality on urban seismic risk analysis was quantified using a testbed group of tall buildings subjected to a fixed ground motion intensity field from an example earthquake scenario consisting of a magnitude 7.0 strike-slip earthquake with an epicenter 21 km away from the center of the group of buildings. The variance of total seismic losses, characterized in terms of the normalized repair cost of all buildings, was shown to depend on building orientations. For example, the case where all buildings had the same orientations, representing a case where streets are laid out in a perfect rectangular grid, had losses with more than double the standard deviation compared to the case where building orientations were sampled randomly from a uniform distribution. Furthermore, for the perfect grid case, the sampled orientation of RotD100 was shown to affect the losses significantly, with the maximum losses tending to occur when the orientation of RotD100 is aligned with that of one of the principal orientations of the buildings and the minimum losses when the orientation of RotD100 was at 45° with respect to the principal orientations of the buildings. Conversely, for the case where building orientations were sampled randomly from a uniform distribution, the orientation of RotD100 had almost no effect on the output losses. Thus, the impact of directionality on seismic losses of a group of buildings depends on the level of similarity of their principal orientations.

The contribution of ground motion directionality to the variance of the total losses was also compared to some other sources of uncertainty considered in the seismic risk analysis, such as those related to variability in structural response modeling and damage assessment, using a variance-based sensitivity analysis. For the case where all buildings have the same principal orientations, the contribution of ground motion directionality to the variance of total losses, which is driven by the sampling of the RotD100 orientation, was found to be more significant than the rest of the sources of uncertainty considered in this study. Moreover, the contribution of ground motion directionality to the variance of total losses increases as more buildings are considered in the analysis when buildings have the same or similar orientations, as is the case in most urban areas. Future studies could explore how ground motion directionality compares to other sources of uncertainty not considered in this study, such as those related to site response, nonlinear structural response, and repair costs associated with different damage states.

The results of this study suggest that ground motion directionality and building orientations could be important in some urban seismic risk analysis, especially when structures with relatively long periods, similar orientations, and close to each other are being considered. Previous urban seismic risk analysis studies have neglected this aspect, usually due to using central tendency measures (e.g., the median, RotD50) to characterize horizontal ground motion intensity. However, the fact that, for the considered group of buildings, some other sources of uncertainty usually considered in seismic risk analysis were shown to be less important in terms of output variance than that associated with ground motion directionality is a compelling argument to start considering this source of uncertainty in future analyses. While this study highlights the importance of ground motion directionality for a somewhat simplified

testbed group of buildings, the quantitative effects are likely to differ in cases with larger spatial extents, heterogeneous building stocks, and varied site conditions. Further study is warranted to perform this type of assessment in real-world conditions.

Acknowledgements

Financial support to the first author to conduct doctoral studies at Stanford University was provided by the National Agency for Research and Development (ANID) / Doctorado Becas Chile under grant 2019-72200307 and the Nancy Grant Chamberlain Fellowship from the Department of Civil and Environmental Engineering at Stanford University. The authors thank Pablo Heresi for some initial discussions, for correcting the CQC procedure by Taghavi and Miranda (2006), and for providing his code to perform regional seismic risk analysis, which was subsequently modified and expanded for this study. The authors also thank James Bantis for the several discussions on the seismic risk analysis framework, and Cristian Cruz and Pablo Heresi for sharing their models on the first translational period and damping ratio fitted with data obtained from hundreds of instrumented buildings.

Data and resources

The global urban street network data developed by Boeing (2022) was obtained from an open data repository on the Harvard Dataverse available at https://doi.org/10.7910/DVN/DC7U0A (last accessed July 2023).

Supplemental material

Supplemental material for this article is available online.

Author note

This research was conducted while Alan Poulos was at the Department of Civil and Environmental Engineering at Stanford University. He is now at the United States Geological Survey and may be contacted at apoulos@usgs.gov.

Declaration of conflicting interests

The authors declared no potential conflicts of interest with respect to the research, authorship, and/or publication of this article.

References

Alonso-Rodríguez A and Miranda E (2016) Dynamic behavior of buildings with non-uniform stiffness along their height assessed through coupled flexural and shear beams. *Bulletin of Earthquake Engineering* 14(12): 3463–3483.

Baker JW and Jayaram N (2008) Correlation of spectral acceleration values from NGA ground motion models. *Earthquake Spectra* 24(1): 299–317.

Beyer K and Bommer JJ (2006) Relationships between median values and between aleatory variabilities for different definitions of the horizontal component of motion. *Bulletin of the Seismological Society of America* 96(4A): 1512–1522.

Boeing G (2019) Urban spatial order: Street network orientation, configuration, and entropy. *Applied Network Science* 4(1): 1–19.

Boeing G (2022) Street network models and indicators for every urban area in the world. *Geographical Analysis* 54(3): 519–535.

Boore DM (2010) Orientation-independent, nongeometric-mean measures of seismic intensity from two horizontal components of motion. *Bulletin of the Seismological Society of America* 100(4): 1830–1835.

Boore DM, Joyner WB and Fumal TE (1997) Equations for estimating horizontal response spectra and peak acceleration from western North American earthquakes: a summary of recent work. *Seismological Research Letters* 68(1): 128–153.

Boore DM, Stewart JP, Seyhan E and Atkinson GM (2014) NGA-West2 equations for predicting PGA, PGV, and 5% damped PSA for shallow crustal earthquakes. *Earthquake Spectra* 30(3): 1057–1085.

Bradley BA and Baker JW (2015) Ground motion directionality in the 2010–2011 Canterbury earthquakes. *Earthquake Engineering & Structural Dynamics* 44(3): 371–384.

Cleveland WS (1979) Robust locally weighted regression and smoothing scatterplots. *Journal of the American Statistical Association* 74(368): 829–836.

Cruz C (2017) *Evaluation of damping ratios inferred from the seismic response of buildings*. PhD Thesis, Stanford University.

Cruz C and Miranda E (2017) Evaluation of the Rayleigh damping model for buildings. *Engineering Structures* 138: 324–336.

Efron B (1982) *The Jackknife, the Bootstrap and Other Resampling Plans*. CBMS-NSF Regional Conference Series in Applied Mathematics. Philadelphia, PA: SIAM.

Filippitzis F, Kohler MD, Heaton TH, Graves RW, Clayton RW, Guy RG, Bunn JJ and Chandy KM (2021) Ground motions in urban Los Angeles from the 2019 Ridgecrest earthquake sequence. *Earthquake Spectra* 37(4): 2493–2522.

Goda K and Hong HP (2008) Estimation of seismic loss for spatially distributed buildings. *Earthquake Spectra* 24(4): 889–910.

Heresi P and Miranda E (2019) Uncertainty in intraevent spatial correlation of elastic pseudo-acceleration spectral ordinates. *Bulletin of Earthquake Engineering* 17: 1099–1115.

Heresi P and Miranda E (2022) Structure-to-structure damage correlation for scenario-based regional seismic risk assessment. *Structural Safety* 95: 102155.

Homma T and Saltelli A (1996) Importance measures in global sensitivity analysis of nonlinear models. *Reliability Engineering & System Safety* 52(1): 1–17.

Hong HP and Goda K (2007) Orientation-dependent ground-motion measure for seismic-hazard assessment. *Bulletin of the Seismological Society of America* 97(5): 1525–1538.

Huang YN, Whittaker AS and Luco N (2008) Maximum spectral demands in the near-fault region. *Earthquake Spectra* 24(1): 319–341.

Lee R and Kiremidjian AS (2007) Uncertainty and correlation for loss assessment of spatially distributed systems. *Earthquake Spectra* 23(4): 753–770.

Park J, Bazzurro P and Baker JW (2007) Modeling spatial correlation of ground motion intensity measures for regional seismic hazard and portfolio loss estimation. In: *10th International Conference on Application of Statistic and Probability in Civil Engineering*. Tokyo, Japan.

Poulos A and Miranda E (2022) Probabilistic characterization of the directionality of horizontal earthquake response spectra. *Earthquake Engineering & Structural Dynamics* 51(9): 2077–2090.

Poulos A and Miranda E (2023a) Effect of style of faulting on the orientation of maximum horizontal earthquake response spectra. *Bulletin of the Seismological Society of America* 113(5): 2092–2105.

Poulos A and Miranda E (2023b) Modification of ground-motion models to estimate orientation-dependent horizontal response spectra in strike-slip earthquakes. *Bulletin of the Seismological Society of America* 113(6): 2718–2729.

Poulos A, Miranda E and Baker JW (2022) Evaluation of earthquake response spectra directionality using stochastic simulations. *Bulletin of the Seismological Society of America* 112(1): 307–315.

Ramirez CM and Miranda E (2009) Building-specific loss estimation methods & tools for simplified performance-based earthquake engineering. Report 171, John A. Blume Earthquake Engineering Center, Stanford, CA.

Rezaeian S, Bozorgnia Y, Idriss IM, Abrahamson N, Campbell K and Silva W (2014) Damping scaling factors for elastic response spectra for shallow crustal earthquakes in active tectonic regions: "average" horizontal component. *Earthquake Spectra* 30(2): 939–963.

Saltelli A, Annoni P, Azzini I, Campolongo F, Ratto M and Tarantola S (2010) Variance based sensitivity analysis of model output. design and estimator for the total sensitivity index. *Computer physics communications* 181(2): 259–270.

Shahi SK and Baker JW (2014) NGA-West2 models for ground motion directionality. *Earthquake Spectra* 30(3): 1285–1300.

Taghavi S and Miranda E (2006) Probabilistic seismic assessment of floor acceleration demands in multi-story buildings. Report 162, John A. Blume Earthquake Engineering Center, Stanford, CA.

Watson-Lamprey JA and Boore DM (2007) Beyond Sa_{GMRotI}: Conversion to Sa_{Arb}, Sa_{SN}, and Sa_{MaxRot}. *Bulletin of the Seismological Society of America* 97(5): 1511–1524.